Measurement of $^{19}F(p,\alpha\gamma)^{16}O$ Reaction Reopens the Fluorine Conundrums in Stars

X. D. Su,[1,2,3] M. La Cognata,[4,*] N. Vukman,[5,6,7] G. G. Rapisarda,[4,8] M. Mazzocco,[2,3,†] A. A. Oliva,[4] L. Roberti,[4,9,10,11] G. L. Zhang,[1,‡] B. Becherini,[5,12] S. Cherubini,[4,8] M. Costa,[4] A. Di Pietro,[4] P. Figuera,[4] G. L. Guardo,[4] M. Gulino,[4,13] S. Hayakawa,[4,14] I. Indelicato,[4,8] M. La Commara,[15,16] L. Lamia,[4,8,17] D. Lattuada,[4,13] S. Palmerini,[5,9,12] R. G. Pizzone,[4,8] S. M. R. Puglia,[4,8] S. Romano,[4,8,17] M. L. Sergi,[4,8] R. Spartà,[4,13] C. Spitaleri,[4,8] D. Torresi,[4] O. Trippella,[5,12] and A. Tumino[4,13]

[1]*School of Physics, Beihang University, Beijing, 100191, China*
[2]*Dipartimento di Fisica e Astronomia, Università di Padova, Padova, 35131, Italy*
[3]*Sezione di Padova, Istituto Nazionale di Fisica Nucleare, Padova, 35131, Italy*
[4]*Laboratori Nazionali del Sud, Istituto Nazionale di Fisica Nucleare, Catania, 95123, Italy*
[5]*Sezione di Perugia, Istituto Nazionale di Fisica Nucleare, Perugia, 06123, Italy*
[6]*Ruder Boskovic Institute, Zagreb, 10001, Croatia*
[7]*Faculty of Science, University of Split, Split, 21000, Croatia*
[8]*Dipartimento di Fisica e Astronomia "Ettore Majorana," Università di Catania, Catania, 95123, Italy*
[9]*Osservatorio Astronomico di Roma, Istituto Nazionale di Astrofisica, Monte Porzio Catone (RM), 00078, Italy*
[10]*Konkoly Observatory, Research Centre for Astronomy and Earth Sciences, Konkoly Budapest, H-1121, Hungary*
[11]*CSFK HUN-REN, MTA Centre of Excellence, Konkoly Budapest, H-1121, Hungary*
[12]*Department of Physics and Geology, University of Perugia, Perugia, 06123, Italy*
[13]*Dipartimento di Ingegneria e Architettura, Kore University, Enna, 94100, Italy*
[14]*Center for Nuclear Studies, The University of Tokyo, Wako-shi (Saitama), 351-0198, Japan*
[15]*Sezione di Napoli, Istituto Nazionale di Fisica Nucleare, Napoli, 80126, Italy*
[16]*Dipartimento di Farmacia, Università di Napoli "Federico II," Napoli, 80131, Italy*
[17]*Centro Siciliano di Fisica Nucleare e Struttura della Materia, Catania, 95123, Italy*

(Received 2 April 2025; revised 20 July 2025; accepted 17 September 2025; published 29 October 2025)

Fluorine abundance in stars is a sensitive indicator of the physical conditions and processes occurring within their interiors. Recent extrapolated results on the $^{19}F(p,\alpha\gamma)^{16}O$ fluorine destruction cross section suggested an increase of the astrophysical factor by several orders of magnitude at astrophysical energies, with profound implications for our understanding of stellar evolution and nucleosynthesis. We have indirectly measured the $^{19}F(p,\alpha\gamma)^{16}O$ cross section using the Trojan horse method, fully covering astrophysical energies with no need of extrapolations. The strength of the 11 keV resonance was extracted and a significant reduction of the reaction rate was determined, compared to previous studies. The analysis of the astrophysical impact suggests that our measurement challenges existing predictions about fluorine and heavier elements' abundances, reigniting unresolved questions in the field.

DOI: 10.1103/cq71-jy7s

Stars are the synthesis site of most atomic elements. In particular, the asymptotic giant branch (AGB) phase of low- and intermediate-mass stars ($M < 8$–9 solar masses—$M_\odot$) is responsible for the production of light elements (carbon, nitrogen, fluorine) through charged-particle reactions, and of heavy elements beyond iron up to bismuth via slow neutron captures (*s* process [1]). Nucleosynthesis in AGB stars is complicated by the activation of several nuclear burning scenarios such as the cool bottom process, the hot bottom burning, and ^{4}He induced reactions in the He-rich intershell region. Such scenarios have been studied throughout the years in several works (see, for instance, Refs. [2–4]). Massive stars ($M > 8$–$9M_\odot$) contributed to the present-day elemental abundances of the Galaxy synthesizing light, intermediate (e.g., oxygen, magnesium, silicon, calcium), and iron-peak (e.g., titanium, iron, nickel) elements through heavy-ion fusions during their lives and their deaths as core-collapse supernovae [5–7]. The first stellar objects formed out of the matter emerged from the big bang (population III stars) were thought to be more massive than $10M_\odot$ or so, up to $\sim 1000M_\odot$. They had a chemical composition mainly dominated by H and He with few traces of D, Li, Be, and B [8]. In this context, α-capture reactions on lithium and boron isotopes could lead to the production of CNO elements, thus impacting our understanding of the cosmological lithium problem. Also, CNO

*Contact author: lacognata@lns.infn.it
†Contact author: marco.mazzocco@pd.infn.it
‡Contact author: zgl@buaa.edu.cn

 © 2025 American Physical Society

breakout may lead to the synthesis of elements heavier than ^{20}Ne (as, for example, calcium) in such pristine stars, now observed in the most ancient stellar objects in our Galaxy [9].

Among all the elements of the periodic table, fluorine (and, specifically, its only stable isotope ^{19}F) is a particularly important one, as it is produced in all the stellar sites discussed above [6,7,10–14] and acts as a separation between the light (Li, Be, B, C, N, O) and intermediate elements (from Ne up to Ca). However, it is also easily destroyed, even at low temperatures of the order of tens of million kelvin ($\leq 4 \times 10^7$ K). Therefore, its abundance bears the footprints of the nucleosynthesis scenarios and can be used as a criterion to constrain astrophysical models.

Despite its importance, fluorine nucleosynthesis is still largely uncertain (as pointed out, for instance, by the NuPECC Long Range Plan 2024 [4]). A possible solution to the fluorine puzzle may arise from advances in experimental nuclear physics. Until the publication of the Nuclear Astrophysics Compilation of Reaction Rates (NACRE) [15], the main contributing channels to the $^{19}\mathrm{F}(p,\alpha)^{16}\mathrm{O}$ cross section were believed to involve the ground and first excited states of ^{16}O. Because of the lack of data, the low-energy astrophysical S factor $S(E) = E\sigma(E)\exp[2\pi\eta]$ [15] was extrapolated using a nonresonant trend, based on the results of an unpublished work (see Ref. [15] for a detailed discussion). The seminal work [16], later corroborated by Ref. [17], showed that the $^{19}\mathrm{F}(p,\alpha)^{16}\mathrm{O}$ reaction, proceeding through the ^{16}O ground state, is endowed with a rich pattern of resonances, especially at center-of-mass energies around 100 keV that correspond to the $^{19}\mathrm{F}(p,\alpha)^{16}\mathrm{O}$ energies of astrophysical relevance for the destruction of fluorine in giant stars [18]. These results triggered the completion of several new studies, which are summarized in Ref. [19], including new indirect and direct measurements (especially underground) and reanalysis of existing data using phenomenological tools such as the R matrix [20].

In particular, recent measurements conducted in the low background environment of the China JinPing Underground Laboratory [21–23], could reach down to about 70 keV center-of-mass energy in the $^{19}\mathrm{F}(p,\alpha\gamma)^{16}\mathrm{O}$ reaction [21,22], mostly populating the ^{16}O second excited state (α_2 channel) [20], and about 180 keV in the $^{19}\mathrm{F}(p,\gamma)^{20}\mathrm{Ne}$ competing channel [23]. Such measurements suggested the occurrence of resonances at low energies, notably, a strong 11 keV resonance has emerged, which may shift the dominance on the rate to the $^{19}\mathrm{F}(p,\alpha\gamma)^{16}\mathrm{O}$ channel around 5×10^7 K [24], the temperatures of interest for fluorine burning in giant stars [18], previously overshadowed by the ground state channel [19]. This resonance strength, while based on extrapolations from data taken at significantly higher energies, leads to a reaction rate for the $^{19}\mathrm{F}(p,\alpha\gamma)^{16}\mathrm{O}$ reaction ~30 times larger than the previous estimates [25] at 5×10^7 K, whereas the $^{19}\mathrm{F}(p,\gamma)^{20}\mathrm{Ne}$ reaction rate is reported to be ~13 times larger than in NACRE [23] at the same temperature. The impact of the occurrence of the 11 keV resonance extends well above 5×10^7 K: sensitivity studies (see Figs. S1 and S2 in Supplemental Material [26]) show that even at 10^8 K its presence causes an increase in the reaction rate by 50% for the $^{19}\mathrm{F}(p,\alpha\gamma)^{16}\mathrm{O}$ and by 20% for the $^{19}\mathrm{F}(p,\gamma)^{20}\mathrm{Ne}$, with possible consequences on nucleosynthesis in other environments, such as early stars [23]. This is also apparent by inspecting Fig. 2 of Ref. [23], where the contribution of the 225 keV resonance is superimposed on a dominant contribution from the 11 keV resonance. Such modifications may significantly impact astrophysical predictions and our understanding of fluorine destruction, given the fact that the $^{19}\mathrm{F}(p,\alpha\gamma)^{16}\mathrm{O}$ rate is giving a major contribution to the total rate [20].

The importance of the low energy region, so far not achieved in direct measurements, has triggered a new indirect measurement using the Trojan horse method (THM) [36,37] focusing on the $^{19}\mathrm{F}(p,\alpha\gamma)^{16}\mathrm{O}$ channel. The THM is an indirect technique developed for the measurement of low-energy nuclear reactions free of the Coulomb barrier suppression and electron screening [38], successfully used in the past decades to measure cross sections of reactions of astrophysical interest (see, e.g., Refs. [36,37] and references therein). It uses a three-body $A(b,cC)s$ reaction to deduce the cross section of the astrophysical $A(x,c)C$ process by assuming a $b = x + s$ configuration and quasifree reaction conditions. The basic features of the method and the details on the experiment are discussed in Supplemental Material [26]. Here, we note that the experiment was carried out at INFN, Laboratori Nazionali del Sud, Catania (Italy). A 55 MeV ^{19}F beam was accelerated by the SMP Tandem accelerator and delivered onto a CD_2 target to induce the reaction $^2\mathrm{H}(^{19}\mathrm{F},\alpha^{16}\mathrm{O})n$. Deuteron was used to transfer a proton to induce the reaction of astrophysical importance, while the neutron acted as the spectator under quasifree conditions. The emitted α and ^{16}O nuclei were detected in coincidence in four silicon position sensitive detectors arranged in a symmetric configuration with respect to the beam axis. The two detectors (A, B) placed at the most forward angles, were equipped with ionization chambers as energy-loss detectors, for particle identification [39]. The other two (C, D), were optimized for α particles detection at less forward angles. A sketch of the experimental setup is presented in Fig. S4 of Supplemental Material [26].

The first step in the data analysis was the selection of the quasifree contribution to the total reaction yield following the procedure in Ref. [40]. Then, a consistency check between the A, C and B, D coincidence pairs (covering almost the same phase-space regions) was performed. Given the perfect agreement, data were summed out and integrated over the experimental angular distributions. The deduced quasifree $^2\mathrm{H}(^{19}\mathrm{F},\alpha^{16}\mathrm{O})n$ cross section for the population of ^{16}O at 6.130 MeV (α_2 channel) is shown in

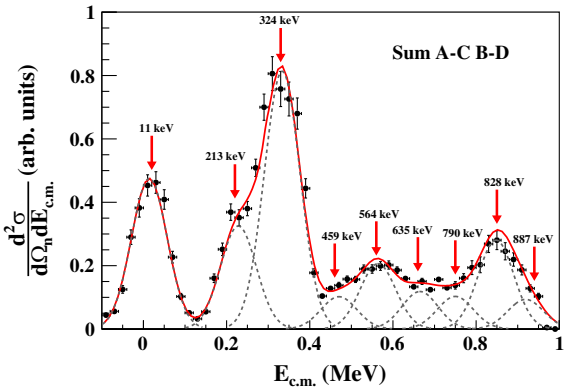

FIG. 1. Experimental cross section and best-fit curve. Quasifree ^{2}H(^{19}F, α^{16}O)n cross section (solid circles) for the population of ^{16}O at 6.130 MeV, that is, the α_2 channel. The red line is a best-fit curve as described in the text, and the dotted lines are the individual contributions. The observed resonances are marked by an arrow.

Fig. 1. This is the channel giving the dominant contribution to the ^{19}F$(p,\alpha\gamma)^{16}$O reaction at astrophysical energies [20]. In the figure, error bars include statistical and angular distribution integration errors. It is important to highlight the role of angular distributions in the data analysis: thanks to the large difference in spin parities of ^{16}O first (0^+) and second (3^-) excited states, the relative contributions of the two channels could be assessed and separated (Table I in Supplemental Material [26]) even if the energy separation of about 80 keV, is below the experimental resolution. Furthermore, the spin parities of the observed resonances in the ^{19}F$(p,\alpha\gamma)^{16}$O reaction were either confirmed or determined for the first time. An extensive discussion of data reduction is provided in Supplemental Material [26].

Using the THM narrow resonance approximation [40], given a constant energy resolution as confirmed by a dedicated Monte Carlo simulation (~100 keV full width at half maximum) including all the experimental effects, the THM resonance strengths N_i equals the areas subtended by the peaks (see Sec. II of Supplemental Material [26] and Ref. [40] for details). According to the procedure in Ref. [40], to extract these values the quasifree cross section was fitted using a sum of Gaussian functions and a linear background (whose contribution was found to be negligible), where the Gaussian centroids are set to the energies reported in the literature [24] and the widths to the simulated energy resolution. The fitting function is displayed as a red line in Fig. 1 (χ^2/n of degrees of freedom $= 2.0$, mostly due to the points above 0.95 MeV), along with the contribution of the single peaks (dotted lines) marked with an arrow and labeled with the resonance energies (see column two in Table I).

The most notable result of the present Letter is the observation of the 11 keV resonance, previously only hypothesized based on an unpublished Ph.D thesis [41] and a transfer reaction [42], whose identification is uncertain due to the large mismatch in the resonance energy. Thanks to the application of the THM, it has been possible to confirm its occurrence and determine its strength. Other resonances, clearly showing up in the cross section, are those at 323.31 keV (used in Refs. [21,22] for normalization) and at 828.17 keV. Given also the accuracy with which their strengths are measured (about 4%), we used them for normalization of the THM resonance strengths [40]. By using two resonances for the normalization, it is possible to reduce the systematic error (as discussed, for instance, in Ref. [43] and references therein). To obtain the resonance strengths in absolute units the THM strengths were corrected to include the Coulomb barrier penetration [40]:

$$(\omega\gamma)_i = \frac{1}{2\pi}\omega_i N_i \frac{\Gamma_{(p^{19}\mathrm{F})_i}}{\frac{d\sigma_{(^{19}\mathrm{F}+d\to n+^{20}\mathrm{Ne}^*_i)}}{d\Omega_n}}, \quad (1)$$

where ω_i is the statistical factor for the ith resonance $(2J_i+1)/[(2J_p+1)(2J_{^{19}\mathrm{F}}+1)]$, J_x the spin of nucleus x, J_i the spin of the ith resonance, N_i the TH resonance strength, and the ratio is calculated in single-particle approximation, so no spectroscopic factors enter the calculation. For the determination of $\Gamma_{(p^{19}\mathrm{F})_i}$ and $d\sigma_{(^{19}\mathrm{F}+d\to n+^{20}\mathrm{Ne}^*_i)}/d\Omega_n$, a standard Woods-Saxon potential was used to describe the nuclear potential well, varying the parameters to assess the systematic error arising from the model dependence, and the plane-wave impulse approximation to describe the proton stripping. It is well known, indeed, that the plane-wave impulse approximation provides a reliable description of the trend of the stripping cross sections but fails to reproduce the absolute values [44]. This is not a problem in our case, since Eq. (1) supplies resonance strengths in arbitrary units. Absolute units have been deduced by scaling the strength of the ith resonance to those of the $\nu = 3$ and $\nu = 8$ ones, according to column 1 of Table I, and taking the weighted average of the two resulting set of strengths.

The present-Letter resonance strengths and total errors are given in Table I, columns 6 and 7, respectively. Total errors include the contribution of the statistical error (at most 4%), the error propagated from the integration of the angular distributions (3% maximum), the normalization error (3%), and the systematic uncertainty due to the model dependence, reaching at most 13%. The latter has been evaluated for each resonance by changing the potential parameters by 10% and propagating the errors. Normalization error is a minor source of uncertainty in the present Letter since the strengths of the resonances used for normalization are known with a ~4% accuracy from direct measurements (Table I). Finally, when taking the weighted average of the resonance strengths deduced for the two different normalizations, it has been considered that only the normalization errors are uncorrelated. The inspection of Table I shows that the 225 keV resonance [23] was not observed in the present

TABLE I. List of the measured strengths and comparison with the literature. Progressive number, resonance energies [15,24], NACRE [15] strengths and their errors, and the present work's strengths and their uncertainties are listed, respectively.

ν	E_i^R (keV)	J^π	$\omega\gamma$ (eV)[a]	$\delta\omega\gamma$ (eV)[a]	$\omega\gamma$ (eV)[b]	$\delta\omega\gamma$ (eV)[b]
(1)	11	1^+	7.5×10^{-29}	3×10^{-29}	1.3×10^{-29}	1.6×10^{-30}
(2)	212.71	2^-	2.2×10^{-2}	4×10^{-3}	2.3×10^{-2}	2.7×10^{-3}
(3)	323.31	1^+	23.1	0.9	24.5	1.8
(4)	459.53	1^+	9.5	0.7	11.4	1.3
(5)	564.42	2^-	50	6	43.7	4.1
(6)	635.31	1^+	88	10	103.4	11.4
(7)	790.53	2^{+c}	27	6	23.7	2.7
(8)	828.17	2^-	785	32	664.2	59.0
(9)	887.14	1^+	452	31	567.1	63.2

[a]Strengths as reported in NACRE [15].
[b]Present-Letter strengths.
[c]Based on the present-Letter angular distributions, we determined a 2^+ spin-parity value.

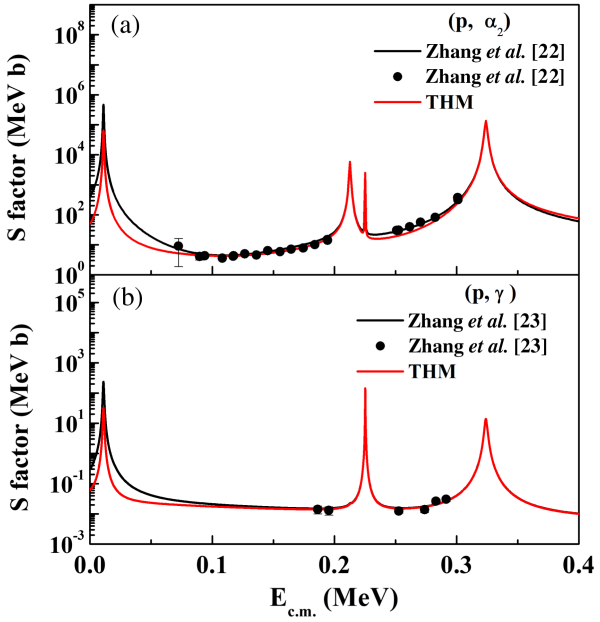

FIG. 2. Astrophysical factors for the $^{19}\mathrm{F}(p,\alpha_2)^{16}\mathrm{O}$ and $^{19}\mathrm{F}(p,\gamma)^{20}\mathrm{Ne}$ reactions. (a) Experimental data from Refs. [21,22] and corresponding R-matrix best fit curve [21], displayed using black circles and a black line, respectively. The astrophysical factor including the present-work 11 keV state resonance strength is shown as a red line. Panel (b) is the same as panel (a), where experimental data and fitting curve are taken from Ref. [23].

Letter, due to its small strength and the effect of the energy resolution [45]. Besides the 11 keV resonance, the analysis was extended to all resonances below 1 MeV to conduct a validity test of our method in the present case (the method has been extensively tested in various systems, see Ref. [43] and references therein). The comparison between the strengths in the literature [15,24] (columns 4 and 5 in Table I) and those deduced from our experiment (columns 6 and 7 in Table I) exhibits a very good agreement for all resonances with the exception of the 11 keV one, with a maximum deviation of 1.8σ.

Focusing on the 11 keV resonance, we confirm the 1^+ spin parity attribution based on our experimental analysis of angular distributions (see Supplemental Material [26] for more details). Our measured strength is 5.8 times smaller than the extrapolated values [15,24], though the corresponding astrophysical factor, renormalized to match the measured resonance strength, is in good agreement with available experimental data, denoting a poor constraint set by direct experimental data taken at energies far from the region of interest. In detail, Fig. 2 shows the comparison between the S factor calculated using the present-Letter strengths of the 11 keV resonance for the $^{19}\mathrm{F}(p,\alpha_2)^{16}\mathrm{O}$ [panel (a)] and $^{19}\mathrm{F}(p,\gamma)^{20}\mathrm{Ne}$ [panel (b)] channels (red line), with the results in Refs. [21–23] (black line for the R-matrix fit, black circles for the experimental data). A very good agreement is generally present, and the deviations in panel (a) are attributed to the lack of details on the R-matrix analysis in Refs. [21,22].

Using the experimental-data-based astrophysical factor from the present experiment, we calculated the reaction rate using the standard formula [Eq. (2) of Ref. [22] and Ref. [46]], inserting the S factors in Fig. 2. By fixing the resonance energies to the ones in the literature, the propagated uncertainty on the reaction rate due to the accuracy in the energy determination is the same as in the literature [22]. The $^{19}\mathrm{F}(p,\alpha_2)^{16}\mathrm{O}$ reaction rate from the present Letter is compared with the one in Ref. [22] in Fig. 3(a), where both rates are divided by the one in Ref. [25] for reference. The THM rate (red band) is generally lower than the one in Ref. [22] (green band) due to the reduced strength of the 11 keV resonance, and its accuracy is significantly improved thanks to the direct observation of the latter. Above about 8×10^7 K, the two rates almost coincide. The comparison with SP00 [25] shows that the role of the 11 keV resonance can be relevant even at higher temperatures, of the order of 10^8 K, since the main difference between Refs. [21,22] and [25] is mostly attributable to the influence of such threshold resonance (see Figs. S1 and S2 in Supplemental Material [26] for a quantitative determination). A similar reduction in the reaction rate is found for the $^{19}\mathrm{F}(p,\gamma)^{20}\mathrm{Ne}$, as it is apparent from the inspection of the S factors in Fig. 2. Figure 3(b) shows the comparison between the present-Letter reaction rate (red band) and the ones in Ref. [23], both divided by the NACRE one [15]. An apparent reduction in the median rate is present, while the uncertainty is significantly reduced at temperatures below 10^8 K thanks to the THM accurate measurement of the 11 keV resonance strength. Since the $^{19}\mathrm{F}(p,\alpha_0)^{16}\mathrm{O}$ and $^{19}\mathrm{F}(p,\alpha_\pi)^{16}\mathrm{O}$ channels (populating $^{16}\mathrm{O}$ ground and first excited state, respectively) are unaffected by the present Letter and provide the largest contribution to the rate

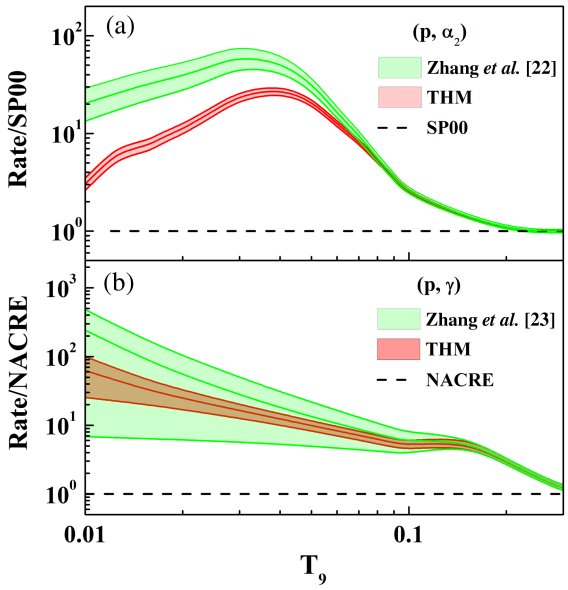

FIG. 3. Present-Letter reaction rates and comparison with the literature. (a) Ratio of the rate from Ref. [22] and the one in Ref. [25] (SP00) used as reference value (green band), compared with the one based on the THM astrophysical factor, also divided by SP00 (red band). The bands highlight the uncertainty range. The temperature is expressed in billion kelvin ($T_9 = T/10^9$ K). (b) Same as panel (a), where the rate from Ref. [23] (green band) and the rate from the present Letter (red band) are divided to the NACRE one [15].

between $\sim 5 \times 10^7$ and $\sim 1.2 \times 10^8$ K [24], a lower ratio of the $^{19}\mathrm{F}(p,\gamma)^{20}\mathrm{Ne}$ rate to the total $^{19}\mathrm{F}(p,\alpha)^{16}\mathrm{O}$ rate (summed over all the exit channels) is obtained. If the NACRE rate [15] is taken as reference, following the same procedure as in Ref. [23], our Letter recommends an enhancement factor of ~ 10 at 5×10^7 K (to be compared with over 13 in Ref. [23]) and of 4.6–6.4 at 10^8 K (to be compared with a factor of 5.4–7.4 in Ref. [23]). While this latter enhancement factor partially overlaps within uncertainties, our measurement-based reaction rate points to a lower ratio even at CNO breakout temperatures. This is because the 11 keV resonance is very strong so it influences the reaction rate even at higher energies.

The recent works [21,22] suggested a significantly higher fluorine destruction rate, approximately 30 times greater than that reported in Ref. [25] at 5×10^7 K. In contrast, the present measurement significantly reduces the contribution of the $^{19}\mathrm{F}(p,\alpha\gamma)^{16}\mathrm{O}$ channel to the total $^{19}\mathrm{F}(p,\alpha)^{16}\mathrm{O}$ rate, resulting in a total rate closer to the NACRE value [15]. Similarly, the revised rate for the $^{19}\mathrm{F}(p,\gamma)^{20}\mathrm{Ne}$ reaction is lower than recent findings, but still exceeds the NACRE results. This leads to a $(p,\gamma)/(p,\alpha)$ reaction rate ratio that is lower than the recent works but higher than NACRE below 3×10^8 K. Therefore, the findings of this Letter have significant implications for astrophysics.

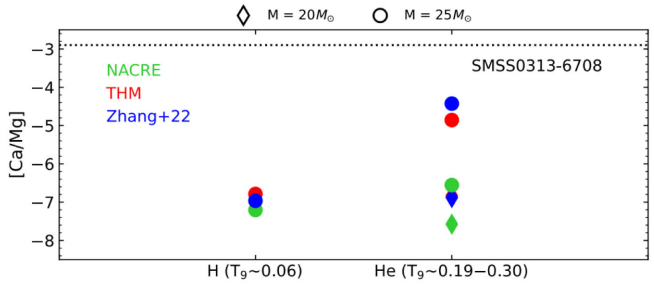

FIG. 4. Impact of present-Letter reaction rate on Pop III stellar models and comparison with SMSS0313-6708. Comparison between stellar yields and SMSS0313-6708 [Ca/Mg] [49] abundance, evaluated at different mass coordinates, to simulate a faint supernova: the base of the hydrogen (H) rich envelope, and the base of the helium (He) shell. The different colors represent yields calculated by means of a different choice for the $^{19}\mathrm{F}$ destruction rates (NACRE for [15], THM for present Letter, and Zhang + 22 for [22,23]). The horizontal dotted line represents the observed $[\mathrm{Ca/Mg}] = -2.9$ in SMSS0313-6708 from [9].

While AGB stars are often considered the primary source of galactic fluorine [10], recent studies [6,11,12,47] have demonstrated that rotating massive stars could have significantly contributed to fluorine production in the early Universe. Rotation induces entanglement between hydrogen- and helium-rich regions, providing the necessary ingredients $(n, p, ^4\mathrm{He}, ^{14}\mathrm{N})$ for fluorine production within the convective He-burning shell. However, the typical temperatures within this shell $(\sim 3 \times 10^8$ K) are likely too high for the revised $^{19}\mathrm{F} + p$ reaction rates to significantly impact fluorine production in these stars. Other potential production sites include core-collapse supernovae (SNeII) via neutrino spallation, Wolf-Rayet stars, and white dwarf mergers ([13], and references therein). However, AGB stars remain the only observationally confirmed source of fluorine [13]. A comprehensive investigation of the impact of these findings on all potential production sites is beyond the scope of this Letter and will be addressed in future studies.

Here, we focus on evaluating the impact of the revised $^{19}\mathrm{F}$ destruction rate on the interpretation of observed $^{40}\mathrm{Ca}$ abundance in the oldest ultra-iron-poor stars. This abundance is attributed to hydrostatic burning in population III stars through the CNO breakout mechanism [9,20]. The $^{19}\mathrm{F}(p,\gamma)^{20}\mathrm{Ne}$ reaction may lead to a leakage of material toward the NeNa mass region, facilitating calcium production and potentially accounting for the observed Ca abundances in the most metal-poor stars known, such as SMSS0313-6708 [9]. Recent studies [23,48] have proposed that CNO breakout, particularly in cases of hydrogen ingestion during the hydrostatic evolution of massive stars, can indeed reproduce observed elemental calcium abundances. However, our findings indicate that the increased $^{19}\mathrm{F}(p,\gamma)^{20}\mathrm{Ne}/^{19}\mathrm{F}(p,\alpha)^{16}\mathrm{O}$ ratio compared to NACRE is insufficient to explain the observed Ca abundance in stars

like SMSS0313-6708, as shown in Fig. 4. This conclusion holds true for both 20 (diamonds) and 25 (circles) solar mass models. The 20 solar mass model experiences no hydrogen ingestion, limiting Ca production to higher temperatures (1.9×10^8 K). The 25 solar mass model experiences the hydrogen ingestion event, causing a merger between the helium and hydrogen convective zones and triggering proton-induced nucleosynthesis in a broader temperature range ($\sim$0.6–1.9×10^8 K). Even including such an ingestion event, the Ca abundance observed in SMSS0313-6708 (dotted line in Fig. 4) is about 2 orders of magnitude higher than the computed models.

In conclusion, the present measurement of the $^{19}\mathrm{F}(p,\alpha\gamma)^{16}\mathrm{O}$ cross section at astrophysical energies, resulting in a diminished channel contribution to the total $^{19}\mathrm{F}(p,\alpha)^{16}\mathrm{O}$ rate, along with the use of a full astrophysical model, challenges the conclusions drawn in Ref. [23] regarding the Ca production in population III stars. Moreover, it is expected to further reduce the impact of fluorine destruction in AGB stars with respect to what is shown in Ref. [24], leaving the fluorine abundance problem unresolved.

Acknowledgments—This work was fully supported by INFN. The authors acknowledge the support of the LNS technical staff during the execution of the experiment. X. D. S. gives thanks to China Scholarship Council for scholarship support she received. G. G. R. acknowledges the "PIAno di inCEntivi per la RIcerca di Ateneo 2020/2022"—Linea di Intervento 3 STARTING GRANT 2020 of the University of Catania. G. L. Z. acknowledges the support by the "111 Center."

Data availability—The data that support the findings of this article are openly available [50].

[1] F. Käppeler, R. Gallino, S. Bisterzo, and W. Aoki, The *s* process: Nuclear physics, stellar models, and observations, Rev. Mod. Phys. **83**, 157 (2011).
[2] S. Palmerini, M. La Cognata, S. Cristallo, and M. Busso, Deep mixing in evolved stars. I. The effect of reaction rate revisions from C to Al, Astrophys. J. **729**, 3 (2011).
[3] H. Jonsson, N. Ryde, G. M. Harper, M. J. Richter, and K. H. Hinkle, Fluorine in the solar neighborhood: Is it all produced in asymptotic giant branch stars?, Astrophys. J. **789**, L41 (2014).
[4] NuPECC, NuPECC long range plan 2024 for European nuclear physics, arXiv:2503.15575.
[5] S. E. Woosley, A. Heger, and T. A. Weaver, The evolution and explosion of massive stars, Rev. Mod. Phys. **74**, 1015 (2002).
[6] M. Limongi and A. Chieffi, Presupernova evolution and explosive nucleosynthesis of rotating massive stars in the metallicity range $-3 \leq [\mathrm{Fe/H}] \leq 0$, Astrophys. J. Suppl. Ser. **237**, 13 (2018).
[7] L. Roberti, M. Limongi, and A. Chieffi, Presupernova evolution and explosive nucleosynthesis of rotating massive stars. II. The supersolar models at $[\mathrm{Fe/H}] = 0.3$, Astrophys. J. Suppl. Ser. **272**, 15 (2024).
[8] B. D. Fields, K. A. Olive, T.-H. Yeh, and C. Young, Big-bang nucleosynthesis after Planck, J. Cosmol. Astropart. Phys. 03 (2020) 010.
[9] S. C. Keller *et al.*, A single low-energy, iron-poor supernova as the source of metals in the star SMSSJ031300.36–670839.3, Nature (London) **506**, 463 (2014).
[10] D. Vescovi, S. Cristallo, S. Palmerini, C. Abia, and M. Busso, Magnetic-buoyancy-induced mixing in AGB stars: Fluorine nucleosynthesis at different metallicities, Astron. Astrophys. **652**, A100 (2021).
[11] L. Roberti, M. Limongi, and A. Chieffi, Zero and extremely low-metallicity rotating massive stars: Evolution, explosion, and nucleosynthesis up to the heaviest nuclei, Astrophys. J. Suppl. Ser. **270**, 28 (2024).
[12] N. Prantzos, C. Abia, M. Limongi, A. Chieffi, and S. Cristallo, Chemical evolution with rotating massive star yields—I. The solar neighbourhood and the s-process elements, Mon. Not. R. Astron. Soc. **476**, 3432 (2018).
[13] I. Indelicato *et al.*, New improved indirect measurement of the $^{19}\mathrm{F}(p,\alpha)^{16}\mathrm{O}$ reaction at energies of astrophysical relevance, Astrophys. J. **845**, 19 (2017).
[14] S. E. Woosley and W. C. Haxton, Supernova neutrinos, neutral currents and the origin of fluorine, Nature (London) **334**, 45 (1988).
[15] C. Angulo *et al.*, A compilation of charged-particle induced thermonuclear reaction rates, Nucl. Phys. **A656**, 3 (1999).
[16] M. La Cognata *et al.*, The fluorine destruction in stars: First experimental study of the $^{19}\mathrm{F}(p,\alpha_0)^{16}\mathrm{O}$ reaction at astrophysical energies, Astrophys. J. Lett. **739**, L54 (2011).
[17] I. Lombardo *et al.*, Toward a reassessment of the $^{19}\mathrm{F}(p,\alpha_0)^{16}\mathrm{O}$ reaction rate at astrophysical temperatures, Phys. Lett. B **748**, 178 (2015).
[18] K. M. Nollett, M. Busso, and G. J. Wasserburg, Cool bottom processes on the thermally pulsing asymptotic giant branch and the isotopic composition of circumstellar dust grains, Astrophys. J. **582**, 1036 (2003).
[19] B. Acharya *et al.*, Solar fusion III: New data and theory for hydrogen-burning stars, Rev. Mod. Phys. **97**, 035002 (2025).
[20] R. J. deBoer, O. Clarkson, A. J. Couture, J. Gorres, F. Herwig, I. Lombardo, P. Scholz, and M. Wiescher, $^{19}\mathrm{F}(p,\gamma)^{20}\mathrm{Ne}$ and $^{19}\mathrm{F}(p,\alpha\gamma)^{16}\mathrm{O}$ reaction rates and their effect on calcium production in Population III stars from hot CNO breakout, Phys. Rev. C **103**, 055815 (2021).
[21] L. Y. Zhang *et al.*, Direct measurement of the astrophysical $^{19}\mathrm{F}(p,\alpha\gamma)^{16}\mathrm{O}$ reaction in the deepest operational underground laboratory, Phys. Rev. Lett. **127**, 152702 (2021).
[22] L. Y. Zhang *et al.*, Direct measurement of the astrophysical $^{19}\mathrm{F}(p,\alpha\gamma)^{16}\mathrm{O}$ reaction in a deep-underground laboratory, Phys. Rev. C **106**, 055803 (2022).
[23] L. Y. Zhang *et al.*, Measurement of $^{19}\mathrm{F}(p,\gamma)^{20}\mathrm{Ne}$ reaction suggests CNO breakout in first stars, Nature (London) **610**, 656 (2022).
[24] L. Y. Zhang, A. Y. López, M. Lugaro, J. J. He, and A. I. Karakas, Thermonuclear $^{19}\mathrm{F}(p,\alpha)^{16}\mathrm{O}$ reaction rate revised

and astrophysical implications, Astrophys. J. **913**, 51 (2021).
[25] K. Spyrou, C. Chronidou, S. Harissopulos, S. Kossionides, T. Paradellis, C. Rolfs, W. H. Schulte, and L. Borucki, Cross section and resonance strength measurements of $^{19}F(p,\alpha\gamma)^{16}O$ at $E_p = 200$–800 keV, Eur. Phys. J. A **7**, 79 (2000).
[26] See Supplemental Material at http://link.aps.org/supplemental/10.1103/cq71-jy7s for a more detailed description of the data analysis, for tabulated data, and for an extensive discussion of the astrophysical calculations, which includes Refs. [27–35].
[27] G. Baur, Breakup reactions as an indirect method to investigate low-energy charged-particle reactions relevant for nuclear astrophysics, Phys. Lett. B **178**, 135 (1986).
[28] M. La Cognata, S. Palmerini, C. Spitaleri, I. Indelicato, A. M. Mukhamedzhanov, I. Lombardo, and O. Trippella, Updated THM astrophysical factor of the $^{19}F(p,\alpha)^{16}O$ reaction and influence of new direct data at astrophysical energies, Astrophys. J. **805**, 128 (2015).
[29] E. Costanzo, M. Lattuada, S. Romano, D. Vinciguerra, and M. Zadro, A procedure for the analysis of the data of a three body nuclear reaction, Nucl. Instrum. Methods Phys. Res., Sect. A **295**, 373 (1990).
[30] D. R. Tilley, H. R. Weller, and C. M. Cheves, Energy levels of light nuclei $A = 16$–17, Nucl. Phys. **A565**, 1 (1993).
[31] L. Lamia, M. La Cognata, C. Spitaleri, B. Irgaziev, and R. G. Pizzone, Influence of the *d*-state component of the deuteron wave function on the application of the Trojan horse method, Phys. Rev. C **85**, 025805 (2012).
[32] I. Lombardo, D. Dell'Aquila, J. J. He, G. Spadaccini, and M. Vigilante, New analysis of $p + {}^{19}F$ reactions at low energies and the spectroscopy of natural-parity states in ^{20}Ne, Phys. Rev. C **100**, 044307 (2019).
[33] R. E. Azuma *et al.*, AZURE: An *R*-matrix code for nuclear astrophysics, Phys. Rev. C **81**, 045805 (2010).
[34] L. Boccioli, L. Roberti, M. Limongi, G. J. Mathews, and A. Chieffi, Explosion mechanism of core-collapse supernovae: Role of the Si/Si-O interface, Astrophys. J. **949**, 17 (2023).
[35] C. L. Fryer, A. Olejak, and K. Belczynski, The effect of supernova convection on neutron star and black hole masses, Astrophys. J. **931**, 94 (2022).
[36] R. E. Tribble, C. A. Bertulani, M. La Cognata, A. M. Mukhamedzhanov, and C. Spitaleri, Indirect techniques in nuclear astrophysics: A review, Rep. Prog. Phys. **77**, 106901 (2014).
[37] A. Tumino, C. A. Bertulani, M. La Cognata, L. Lamia, R. G. Pizzone, S. Romano, and S. Typel, The Trojan Horse method: A nuclear physics tool for astrophysics, Annu. Rev. Nucl. Part. Sci. **71**, 345 (2021).
[38] H. J. Assenbaum, K. Langanke, and C. Rolfs, Effects of electron screening on low-energy fusion cross sections, Z. Phys. A **327**, 461 (1987).
[39] A. Badalà *et al.*, Trends in particle and nuclei identification techniques in nuclear physics experiments, Riv. Nuovo Cimento **45**, 189 (2022).
[40] M. La Cognata *et al.*, A novel approach to measure the cross section of the $^{18}O(p,\alpha)^{15}N$ resonant reaction in the 0–200 keV energy range, Astrophys. J. **708**, 796 (2010).
[41] M. Kious *et al.*, Ph. D. thesis, Universite de Paris XI, 1990.
[42] R. R. Betts, H. T. Fortune, and R. Middleton, Structure of ^{20}Ne: The $^{19}F(^3He, d)^{20}Ne$ reaction, Phys. Rev. C **11**, 19 (1975).
[43] M. La Cognata *et al.*, A new reaction rate of the $^{27}Al(p,\alpha)^{24}Mg$ reaction based on indirect measurements at astrophysical energies and implications for ^{27}Al yields of intermediate-mass stars, Astrophys. J. **941**, 96 (2022).
[44] E. I. Dolinsky *et al.*, Peripheral-model approach to stripping into resonant states, Nucl. Phys. **A202**, 97 (1973).
[45] M. La Cognata, R. G. Pizzone, J. José, M. Hernanz, S. Cherubini, M. Gulino, G. G. Rapisarda, and C. Spitaleri, A Trojan Horse approach to the production of ^{18}F in novae, Astrophys. J. **846**, 65 (2017).
[46] C. Iliadis *et al.*, *Nuclear Physics of Stars* (Wiley, Weinheim, 2007).
[47] N. Prantzos *et al.*, On the origin of the Galactic thin and thick discs, their abundance gradients and the diagnostic potential of their abundance ratios, Mon. Not. R. Astron. Soc. **523**, 2126 (2023).
[48] O. Clarkson and F. Herwig, Convective H–He interactions in massive population III stellar evolution models, Mon. Not. R. Astron. Soc. **500**, 2685 (2021).
[49] [Ca/Mg] is defined as $\log_{10}(X_{Ca}/X_{Mg})_{star}$—$\log_{10}(X_{Ca}/X_{Mg})_{sun}$, where X_{Ca} and X_{Mg} are the elemental abundances in mass fraction of Ca and Mg in the ejecta of the stellar model under consideration ("star" subscript) and in the sun ("sun" subscript).
[50] The data are available in Supplemental Material [26]. Raw data are available from the authors upon reasonable request.